Supporting Information

Stachowiak et al. 10.1073/pnas.0913306107

SI Text

Supporting Analysis. The force required to pull a tubule from a lipid vesicle mechanically can be expressed as follows Eq. **S1**, where C_0 is the membrane spontaneous curvature (1).

$$f_{\text{tubule}} = 2\pi(\sqrt{2\kappa\sigma} - \kappa C_0) \qquad \textbf{[S1]}$$

When bound proteins crowd the outer surfaces of lipid domains they likely increase the spontaneous curvature of the domain, causing it to bend outward, a manifestation of the bilayer couple model (2). Most tubules are fully extended, consuming the entire domain area, suggesting that protein attachment deforms the entire domain at once, increasing the tubule aspect ratio as more proteins attach rather than extending a tubule of constant diameter (Fig. 5*A*). When the spontaneous curvature, C_0, increases to approximately, $\sqrt{\sigma/2\kappa}$, expression Eq. **S1** predicts that tubule formation will occur spontaneously, with no applied force. For a bending rigidity, $\kappa \sim 1 \times 10^{-18}$ J of the gel-phase lipid tubule (3) and an initial tension, σ, of $\sim 5 \times 10^{-5}$ J/m^2, this minimum curvature corresponds to a maximum tubule radius, $1/C_0$, of approximately 200 nm, which is somewhat larger than the largest tubule radius we calculate.

From this analysis, which applies when membrane tension remains constant during tubule formation due to the availability of excess membrane area, we might expect all tubules to have the same radius, a function of the local variables. If all tubules had the same radius, tubule length should increase as the square of the vesicle radius assuming fixed fractional domain area. Instead, we observe a clear linear increase in tubule length with domain area (Fig. 4*B*), implying that tubule diameter is proportional to vesicle diameter (Fig. 4*C*, Eq. 1). The following analysis suggests a possible explanation for this linearly coupled behavior.

Spherical vesicles contain the maximum volume for their surface area such that deformation of the lipid domain into a tubule must be accommodated by an area dilation $A_R = A_{\text{final}}/A_{\text{initial}} \geq 1$, if encapsulated volume is conserved. GUVs are known to contain extra area in the form of multiscale membrane fluctuations, $A_R \sim 1.02$–1.03 (4). These reservoirs can accommodate deformation to vesicle surfaces with modest increases in membrane tension (4). Additional membrane area dilations can be achieved by straining the membrane to reduce the lipid packing density. We apply continuity constraints to the vesicle deformation process to examine how these processes could impact the deformed vesicle geometry.

Eq. **S2** states that the vesicle volume is conserved, where R_0 is the initial vesicle radius, R_A is the final vesicle radius, R_T is the tubule radius, and L_T is the tubule length.

$$\frac{4}{3}\pi R_0^3 = \frac{4}{3}\pi R_A^3 + \pi R_T^2 L_T \qquad \textbf{[S2]}$$

Eq. **S3** states that the initial vesicle surface area, multiplied by A_R is equal to the final surface area of the vesicle and attached tubule.

$$4\pi A_R R_0^2 = 4\pi R_A^2 + 2\pi R_T L_T \qquad \textbf{[S3]}$$

Eq. **S4** states that the surface area of the undeformed lipid domain, which takes up a fixed percentage, A_D, of the undeformed vesicle surface, is equal to the surface area of the lipid tubule.

$$4\pi A_D R_0^2 = 2\pi R_T L_T \qquad \textbf{[S4]}$$

Combining Eqs. **S2**–**S4** to eliminate L_T and R_0, we find expression Eq. **S5**, which relates the radius of the deformed vesicle, R_A, to the tubule radius, R_T, in terms of the parameters, A_R, and A_D.

$$\frac{R_T}{R_A} = \frac{2}{3}\frac{(1-(A_R-A_D)^{3/2})}{A_D(A_R-A_D)^{1/2}} \sim \text{constant} \qquad \textbf{[S5]}$$

Examining **[S5]** it is clear that any deformation of the vesicle for which A_R is constant will result in a constant ratio R_T/R_A. For the observed R_T/R_A ratios for $A_D \sim 0.056$, an area dilation of $\sim$1.05 could fully accommodate the vesicle deformation. Area dilations of this magnitude have been recorded previously (4) but may approach vesicle lysis for some lipid compositions. Since the domain area is fixed, the ratio of tubule length to vesicle radius is also constant **[S6]**.

$$\frac{L_T}{R_A} \sim \frac{2A_D}{(A_R-A_D)\frac{R_T}{R_A}} \sim \text{constant} \qquad \textbf{[S6]}$$

Formation of tubules with a constant L_T/R_A aspect ratio is expected when the area dilation, A_R, is constant for a given lipid composition. We now examine how the physical process of membrane deformation by protein binding could define a constant area dilation.

It is likely that a global limitation on vesicle deformation arises from the finite binding energy between the protein histidine tag and the lipid membrane. This energy limits the work the protein can do in bending the membrane. The free energy, F, of the lipid vesicle surface can be expressed as follows Eq. **S7**, where A_V is the vesicle surface area, σ is the membrane tension, V is the vesicle volume, p is the pressure differential across the membrane, κ is the membrane bending energy, and H is the mean curvature of the membrane (5).

$$F = \sigma A_V - pV + \int \frac{\kappa}{2}(2H)^2 dA \cong \sigma A - pV + \kappa\pi\frac{L_T}{R_T} \qquad \textbf{[S7]}$$

As the vesicle deforms, the membrane tension will increase. From an equilibrium force balance on the vesicle cross section, pressure will increase with membrane tension Eq. **S8**.

$$p \cong \frac{2\sigma}{R} \qquad \textbf{[S8]}$$

The finite energy of protein binding to the lipid membrane, ΔG, limits the membrane tension that protein binding can create. After the lipid domain is fully covered with bound proteins, additional proteins must stretch the membrane by an amount equal to the area they occupy on the membrane surface in order to bind. As the membrane tension approaches the limiting tension, the first two terms of Eq. **S7**, which depend on tension, will increase such that the third term, the curvature energy, may likely be neglected, leading to Eq. **S9**.

$$F \approx \frac{4}{3}\sigma_{\max}\pi R^2 = \frac{\Delta G A_D A_V}{A_P} \qquad \textbf{[S9]}$$

For example, the smallest vesicles we measure, about 1 μm in radius, will have a curvature energy of about 1×10^{-16} J assuming $\kappa \sim 1 \times 10^{-18}$ J for the gel-phase lipid tubule (3) and 10% DSIDA content ($A_D \sim 0.056$) in the membrane. This curvature energy

represents about 1% of the free energy from protein binding if the binding energy, ΔG, of 6-histidine to DSIDA is approximately 1×10^{-19} J, and A_P is approximately 9 nm^2 for the protein his-GFP.

From [**S9**] we find an expression for the maximum tension [**S10**].

$$\sigma_{\max} \approx \frac{3\Delta G A_D}{A_P} \approx E \frac{\delta A}{A_V}\bigg|_{\sigma} \qquad \textbf{[S10]}$$

Once the extra lipid area from fluctuations is removed at relatively low tension, tension will increase proportionally to the area strain, where E, the elastic modulus for direct area expansion of the membrane, is the constant of proportionality [**S10**]. Therefore, we predict that protein binding to the lipid domain could cause a maximum membrane tension that is constant for a given vesicle composition. Making reasonable estimates for the constants (above), we find a maximum tension of the order 1×10^{-3} J/m^2, about two orders of magnitude above the initial membrane tension and one order of magnitude below the lytic tension (6). This tension will cause a modest increase in pressure that we estimate will push out an insignificant amount of fluid in balance with the osmotic pressure. A constant membrane tension will lead to constant area dilations of approximately 1–2% based on an area extension modulus of about 150×10^{-3} J/m^2 (4) for the fluid portion of the membrane. This constant dilation will lead to tubules with constant L/R_0 ratio. Further, expression [**S9**] predicts that the energy invested in membrane bending increases with the protein binding energy and decreases with the protein size because proteins of larger size limit the number of binding interactions, which supply the energy for bending. This prediction could explain our observation that proteins of smaller molecular weight form tubules more frequently. This analysis assumes that the domain boundary has sufficient line energy to resist dissolution as proteins crowd the domain (7).

Our simple analysis suggests that a constant membrane tension determined by protein binding to a lipid domain is consistent with the constant L/R_0 ratio we observe. Quantitative prediction of L/R_0 depends on precise knowledge of the constants, A_P, E, and ΔG, which are unknown and likely vary with the vesicle composition. However, L/R_0 is likely limited by the finite binding energy, ΔG, which will produce a fixed maximum tension and area dilation, leading to a fixed L/R_0 ratio. Therefore our analysis, suggests that the system is governed by a global tension limit. We predict that this limit is constant for a given vesicle composition and depends on protein-membrane binding energy, fractional domain size, and protein size.

Supporting Methods. ***GUV slide preparation.*** After electroformation, vesicles were diluted, exposed to his-tagged proteins and prepared for imaging. In all cases, the vesicles were diluted (2-20X) in a solution containing 200 μM $CuCl_2$ in 50 mM MOPS buffer. This solution was adjusted to an osmolarity of approximately 350 milliosmole (mOsm) by adding 2 M glucose solution. His-tagged proteins were added to the vesicle mixture at concentrations ranging from 20 nM to 2 μM as described in *Results*. In all cases, vesicles were observed in small sealed disposable chambers composed of cover slips and spacers made from double-sided tape. Lipid tubule formation began immediately upon addition of his-tagged proteins and was largely complete after a few minutes. However, samples were allowed to rest 1 h after preparation to give tubes time to form and allow vesicles to sink (in less dense glucose solution) to the chamber bottom for imaging and counting.

Microscopy. The vesicles were observed using epifluorescence, confocal, and differential interference contrast (DIC) microscopy. Images appearing in Figs. 1, 2, and 4 were taken using a 100X oil immersion objective. Images from which tube formation probabilities were calculated were taken using a 60X oil immersion objective in epifluorescence and looked similar to Fig. 2*B*. Two-color confocal images were taken using a Solamere spinning disk confocal system equipped with a Cascade II cooled CCD camera on an Zeiss AxioObserver inverted microscope at 100X. Two-color epifluorescent images were taken on an Olympus inverted microscope using an Andor cooled CCD camera. DIC images overlaid with single color epifluorescence images were taken on a Zeiss AxioObserver inverted microscope equipped with a Cool Snap CCD camera.

Calculation of tubule formation frequency. The frequency of tube formation was calculated as the number of tubes divided by the number of vesicles within the same field of view. For each reported value, results from 8–11 fields of view were averaged. The scale bar represents the first standard deviation of these measurements. Within a given field of view, tubes and vesicles were counted by manually analyzing sets of images from a Z-scan beginning at the plane of the cover slip and extending at least 100 μm into the sample, which included nearly all GUVs and corresponded to the working limit of the objective. In cases where the number of tubes was much less than the number of vesicles, the tubes were often counted over the entire field of view, while vesicles were counted over a subsection of the field. In these instances, the total number of vesicles in the field of view was estimated by assuming that the number of vesicles per unit area remained constant over the entire field.

Formation of supported lipid bilayers. Small unilamellar vesicles were formed by dissolving desired lipids in chloroform to a final concentration of about 2 mM. In a conical flask, the chloroform solution was evaporated under rotary evaporation, leaving behind a smooth lipid film. The film was further dried under vacuum overnight and then rehydrated in 5 mL of 50 mM phosphate buffer for at least 15 min. The rehydrated film was vigorously swirled to fully suspend the lipid film. The lipid solution was then sonicated with a tip sonicator at a power of 10 watts under a constant flow of nitrogen for a total of 12 min (3 segments, 4 min long each, separated by 2 min rest periods). The sonicated solution was then centrifuged (16,000 x *g*, 20 min) and the supernatant filtered through a 0.2 μm GHP filter. Glass cover slips were cleaned by immersion in piranha solution (25% (30% aqueous H_2O_2)/H_2SO_4). [Caution, piranha is extremely corrosive and dangerous to the skin, eyes, and lungs.]

Fluorescence correlation spectroscopy. Fluorescence correlation spectroscopy was performed on supported lipid bilayer samples prepared as described above. The BODIPY lipid label was used as the fluorophore at a concentration of 0.0025 mol %. Measurements were made using 532 nm excitation through a 100X oil immersion objective. A custom photon time-stamping system was used to collect the data and the autocorrelation curves were calculated offline from the time-stamped photon list data. The autocorrelations were fit to extract diffusion constants using standard forms for correlation functions in two dimensions with one or two diffusion components.

Imaging of lipid tubule growth. Lipid tubule growth begins immediately upon addition of his-tagged proteins. Therefore, to watch tubule growth, protein addition must occur only after the vesicle solution is setup on the microscope and ready to be imaged. For these experiments, an open chamber design was used so that the protein solution could be added during imaging. The chamber consisted of a silicone rubber sheet (~3 mm thick) with a 5 mm diameter hole centered in the middle. The rubber was adhered with pressure to a glass cover slip to form an open well.

The vesicle solution was mixed with dilution buffer (described above) and pipetted into the well. Vesicles were given at least 15 min to settle on the cover slip surface. Imaging began at a rate of one set of frames per second, where each set included one epifluorescent image of GFP and one DIC image of the vesicles. The protein solution was gently added to the top of the well by pipette to minimize translation of the vesicles. Adsorption of protein to the vesicle membranes began when protein diffused to the vesicle surfaces, approximately 0.5–2 min following addition of the protein solution, and coincided with membrane deformation.

Measurement of vesicle dimensions. We measured vesicle diameters and the lengths of individual lipid tubules connected to vesicles from confocal image scans perpendicular to the image plane. For accurate measurement of tubule length, we only measured tubules clearly attached to vesicles where the entire domain had been converted into the tubule, the tubule was lying parallel to the imaging plane, and the vesicle maximum diameter was clearly focused and resolved. The average area of DSIDA-rich domains as a percentage of total vesicle surface area was estimated from measurements of the maximum radius of the dark domain region in confocal image stacks. The approximate fractional domain areas were somewhat smaller than the molar fractions of DSIDA in the vesicles. Based on the apparent very low binding of protein to nondomain regions of the GUV, we believe that the nondomain regions contain very little DSIDA. Therefore, we assume that the aerial density of lipids within the lipid domain must be somewhat higher than that of the surrounding fluid phase region to explain the difference between domain area fraction and molar fraction. The higher density of gel-phase lipid membranes has been reported in the literature for 1,2-dimyristoyl-sn-glycero-3-phosphocholine (DMPC), where fluid membranes have a spacing of about 65 nm^2/lipid (8) and gel membranes have a density of about 45 nm^2/lipid (9).

1. Derenyi I, et al. (2007) *Controlled Nanoscale Motion* (Springer Berlin, Heidelberg), 711:141–159.
2. Sheetz MP, Singer SJ (1974) Biological membranes as bilayer couples, A molecular mechanism of drug-erythrocyte interactions. *Proc Nat'l Acad Sci U S A* 71:4457–4461.
3. Lee C, Lin W, Wang J (2001) All-optical measurements of the bending rigidity of lipid-vesicle membranes across structural phase transitions. *Physical Review E* 64:020901-1–020901-4.
4. Evans E, Rawicz W (1990) Entropy-driven tension and bending elasticity in condensed-fluid membranes. *Phys Rev Lett* 64:2094–2097.
5. Derenyi I, Julicher F, Prost J (2002) Formation and interaction of membrane tubes. *Phys Rev Lett* 88:238101-1–238101-4.
6. Evans E, Heinrich V, Ludwig F, Rawicz W (2003) Dynamic tension spectroscopy and strength of biomembranes. *Biophysical Journal* 85:2342–2350.
7. Owicki JC, McConnell HM (1979) Theory of protein-lipid and protein-protein interactions in bilayer membranes. *Proc Nat'l Acad Sci U S A* 76:4750–4754.
8. Petrache HI, Dodd SW, Brown MF (2000) Area per lipid and acyl length distributions in fluid phosphatidylcholines determined by (2)H NMR spectroscopy. *Biophys J* 79:3172–3192.
9. Tristram-Nagle S, Liu Y, Legleiter J, Nagle JF (2002) Structure of gel-phase DMPC determined by X-ray diffraction. *Biophys J* 83:3324–3335.

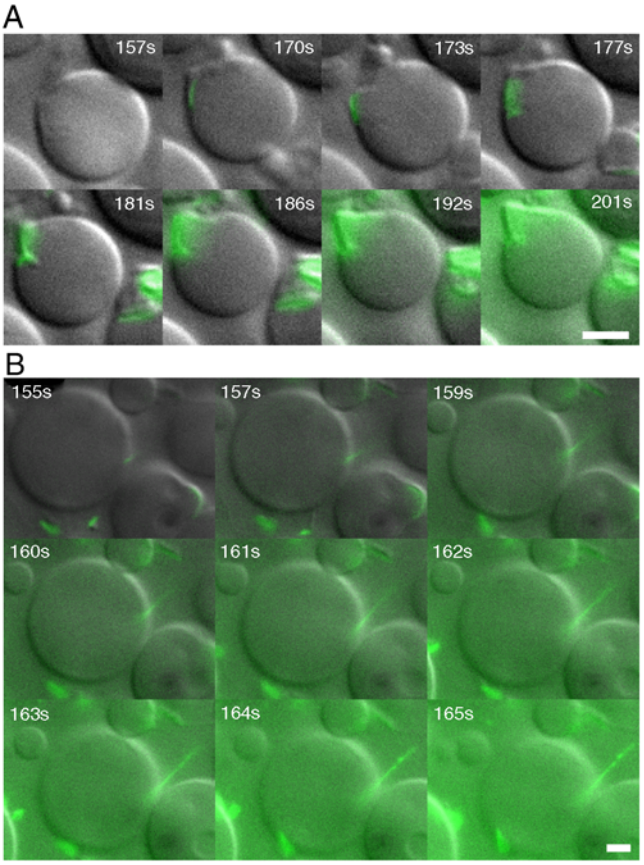

Fig. S1. Lipid membranes are deformed by protein attachment and crowding. Merge of differential interference contrast and GFP epifluorescence images. The times on the frames represent seconds following addition of the GFP protein. (*A*) Deformation of a lipid domain into a bud structure. (*B*) Growth of a lipid tubule from a lipid vesicle surface. (Scale bar, 5 μm).

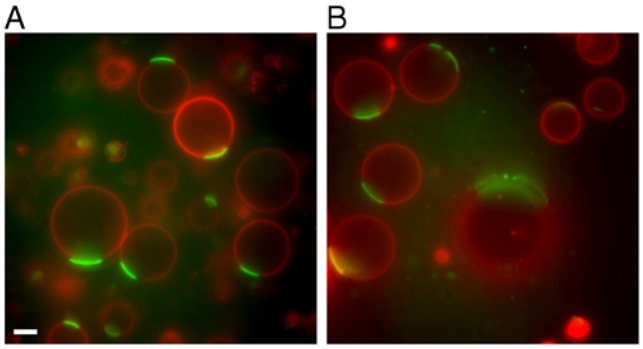

Fig. S2 The matrix lipids DOPC and DLPC do not increase tubule formation in comparison to POPC. Merged epifluorescent images (BODIPY (red), GFP (green)) of vesicles consisting of (*A*) 10% DSIDA / 89.7% DOPC / 0.3% BOPDIPY and (*B*) 10% DSIDA / 89.7% DLPC / 0.3% BOPDIPY. All vesicles exposed to 2 μM his-GFP. Imaging was performed with a 60X oil immersion objective. (Scale bar, 10 μm).

Fig. S3 Soy PE is highly soluble in DSIDA-rich domains. Epifluoresce images (60X oil immersion) of GFP fluorescence from vesicles containing 10% DSIDA / 40% Soy PE in a POPC matrix. In comparison to vesicles that did not contain Soy PE (compare to Fig. 2*A*) the protein labeled lipid domain takes up a significantly larger portion of the vesicle surface area, about 50% in comparison to <10% without Soy PE. This large increase in the domain size upon inclusion of Soy PE likely indicates that Soy PE is highly soluble in the DSIDA-rich domain, enlarging it. All vesicle exposed to 2 μM his-GFP. (Scale bar, 5 μm).

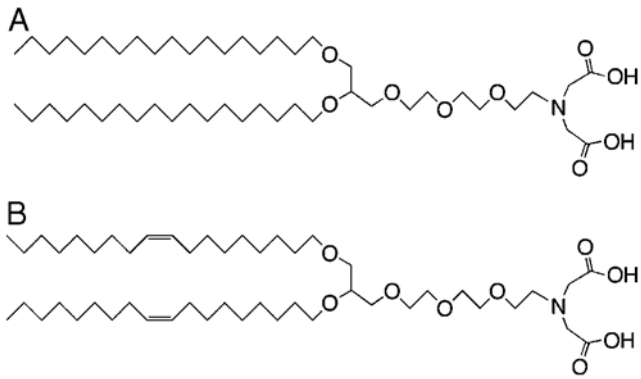

Fig. S4 Chemical structures of (*A*) DSIDA (Distearylglycero triethyleneglycyl iminodiacetic acid), and (*B*) DOIDA (Dioleylglycero triethyleneglycyl iminodiacetic acid), lipid molecules.

Table S1. Micron-scale domains persist to lower concentrations of DSIDA in GUVs consisting of DSIDA / POPC in comparison to those consisting of DSIDA / DPHPC. All GUVs contained 0.3 mol% BODIPY.

DSIDA content	Domain area (POPC matrix)	Domain area (DPhPC matrix)
7.5%	4.4% ± 1.3%	4.6% ± 2.7%
6%	3.0% ± 0.7%	2.0% ± 1.1%
4.5%	1.7% ± 0.3%	No micron-scale domains
3%	0.7% ± 0.4%	No micron-scale domains

All measurements were made in the absence of protein.